Front. Optoelectron. 2017, 10(1): 70–79
DOI 10.1007/s12200-017-0660-5

RESEARCH ARTICLE

Cross-correlation frequency-resolved optical gating scheme based on a periodically poled lithium niobate waveguide for an optical arbitrary waveform measurement

Chenwenji WANG, Peili LI (✉), Yuying GAN, Di CAO, Xiaozheng QIAO, Chen HE

School of Optoelectronic Engineering, Nanjing University of Posts and Telecommunications, Nanjing 210023, China

Abstract This study proposes a novel scheme of a cross-correlation frequency-resolved optical gating (X-FROG) measurement for an optical arbitrary waveform (OAW) based on the sum frequency generation (SFG) effect of a periodically poled lithium niobate (PPLN) waveguide. Based on the SFG effect and combined with the principal component generalized projects algorithm on a matrix, the theory model of the scheme is established. Using Matlab, the proposed OAW measurement X-FROG scheme using the PPLN waveguide is simulated and studied. Simulation results show that a rectangular pulse is a suitable gate pulse because of its low errors. Moreover, the increased complexity of OAW and phase mismatch decrease measurement accuracy.

Keywords optical arbitrary waveform (OAW) measurement, periodically poled lithium niobate (PPLN), cross-correlation frequency-resolved optical gating (X-FROG)

1 Introduction

Optical arbitrary waveform generation (OAWG) techniques can be used to break the speed and bandwidth bottlenecks of electronic technologies for waveform generation [1–6].

In developing OAWG, the ability to characterize accurately optical arbitrary waveform (OAW) plays an important role in many fields of science and technology. The main techniques for optical arbitrary waveform measurement include dual-quadrature spectral interferometry, dual-comb electric-field cross-correlation, and frequency-resolved optical gating (FROG). An advantage of the dual-quadrature spectral interferometry technique with respect to the characterization of OAWG signals is that spectral resolution requirements are reduced to an approximate frequency spacing of the comb, in which the high power pulses required by FROG are not always readily available [7–11]. The dual-comb electric-field cross-correlation technique is linear and provides high measurement sensitivity and fast (tens of microseconds) data acquisition [12–14]. Among these methods, FROG uses time and frequency domains to measure intensity and phase of optical waveforms with a sub-femtosecond resolution. This process realizes phase reconstruction for the track diagram of a generated signal light, which measures an OAW based on the nonlinear effect between the OAW and an adjustable delayed gate pulse [15–23].

Periodically poled lithium niobate (PPLN) is characterized by the advantages of ultra-fast response, no excess noise, and complete transparency, among others [24,25]. Optical frequency conversion based on the nonlinear optical interactions in PPLN is widely used in burgeoning fields of quantum information processing and spectroscopy. Moreover, the PPLN waveguide has a wealth of second-order nonlinear effect, including second-harmonic generation (SHG), sum-frequency generation (SFG), and difference-frequency generation. Here, we used PPLN as the nonlinear medium based on its SHG effect.

We proposed a novel cross-correlation frequency resolved optical gating (X-FROG) measurement system for OAWs. The theory model of the scheme was established based on the SFG effect of the PPLN waveguide combined with the principal component generalized project (PCGP) algorithm based on a matrix. The proposed X-FROG scheme using the PPLN waveguide was studied using Matlab. Measurement of intensity and phase of OAW were obtained through numerical simulation.

Received June 7, 2016; accepted December 16, 2016

E-mail: lipl@njupt.edu.cn

2 Operation principle

Figure 1 shows the schematic diagram of the X-FROG measurement for OAWs using a PPLN waveguide. A gate pulse generated from a continuous-wave laser source was modulated with a Mach-Zehnder modulator, followed by a variable delay. The OAW to be measured and the gate pulse were coupled into the PPLN waveguide. The OAW and the gate pulse propagated in the PPLN waveguide, thus resulting in the SFG effect and generating the signal pulse. After filtering the signal pulse out by a tunable filter, the X-FROG trace of intensity versus frequency and delay was recorded by a charge-coupled device and an optical spectrum analyzer. Finally, the intensity and phase of OAW were retrieved by the PCGP algorithm based on a matrix.

3 Theory model

Assume that the optical field of an incident arbitrary waveform to be measured and the gate pulse are $E_{\mathrm{P}}(t)$ and $E_{\mathrm{G}}(t)$, respectively. After transmitting through variable delay, the optical fields of these two pulses are expressed as $E_{\mathrm{P}}(t)$ and $E_{\mathrm{G}}(t,\tau)$, respectively. Then the sum frequency effect is occurred in PPLN, and a new signal pulse $E_{\mathrm{sig}}(t,\tau)$ is generated due to interaction.

The value of the total wave vector mismatch can be expressed as

$$\Delta k_{\mathrm{SFG}} = \Delta K_{\mathrm{SF}} - 2\pi/\Lambda, \tag{1}$$

where ΔK_{SF} is the phase mismatch factor in the process of SFG among arbitrary waveform, gate pulse, and signal pulse. The phase shift of $(-2\pi/\Lambda)$ is proposed by designing an appropriate quasi-phase-matched period (Λ) to maintain the value of $\Delta k_{\mathrm{SFG}} = 0$.

Therefore, $E_{\mathrm{sig}}(t,\tau)$ can be expressed as

$$E_{\mathrm{sig}}(t,\tau) = E_{\mathrm{P}}(t)\cdot\frac{\mathrm{i}\cdot\omega_{\mathrm{G}}L}{2cn_{\mathrm{G}}}d_{\mathrm{NL}}\cdot E_{\mathrm{G}}(t,\tau), \tag{2}$$

where L is the nonlinear length, d_{NL} is the nonlinear optical hyperpolarizability value in the PPLN waveguide, and n_{G} is the refraction of the gate pulse in the waveguide.

Using Fourier transform, the frequency spectrum of the signal pulse can be written as

$$E_{\mathrm{sig}}(\omega,\tau) = \int_{-\infty}^{+\infty} E_{\mathrm{P}}(t)\cdot\frac{\mathrm{i}\cdot\omega_{\mathrm{G}}L}{2cn_{\mathrm{G}}}d_{\mathrm{NL}}\cdot E_{\mathrm{G}}(t,\tau)\exp(-\mathrm{i}\omega t)\mathrm{d}t. \tag{3}$$

$I_{\mathrm{FROG}}(\omega,\tau)$ is the expression of X-FROG trace:

$$\begin{aligned} I_{\mathrm{FROG}}(\omega,\tau) &= |E_{\mathrm{sig}}(\omega,\tau)|^2 \\ &= \left|\int_{-\infty}^{+\infty} E_{\mathrm{P}}(t)\cdot\frac{\mathrm{i}\cdot\omega_{\mathrm{G}}L}{2cn_{\mathrm{G}}}d_{\mathrm{NL}}\cdot E_{\mathrm{G}}(t,\tau)\exp(-\mathrm{i}\omega t)\mathrm{d}t\right|^2. \end{aligned} \tag{4}$$

The intensity and phase of OAW to be measured can be retrieved from the measured X-FROG trace by the PCGP algorithm [24,25].

To characterize the complexity of OAWs, a precise root mean square (rms) time-bandwidth product (TBP) [26] is introduced:

$$\begin{aligned} &\mathrm{TBP}_{\mathrm{rms}} = t_{\mathrm{rms}}\omega_{\mathrm{rms}}, \\ &t_{\mathrm{rms}}^2 = \langle t-\langle t\rangle^2\rangle = \langle t^2\rangle - \langle t\rangle^2, \\ &\langle t^2\rangle = \int_{-\infty}^{\infty} t^2 I(t)\mathrm{d}t, \\ &\omega_{\mathrm{rms}}^2 = \int_{-\infty}^{\infty} E_{\mathrm{P}}'(t)^2\mathrm{d}t + \int_{-\infty}^{\infty} E_{\mathrm{P}}(t)^2\phi'(t)\mathrm{d}t, \end{aligned} \tag{5}$$

where $I(t)$ is the normalized intensity, t_{rms} is the rms temporal width, ω_{rms} is the rms spectral width, and $\phi(t)$ is the temporal phase.

Generally, when the value of TBP is below 5, the OAW is simple. When the value of TBP is between 5 and 30, the pulse is relatively complex. When the value of TBP is greater than 30, the pulse is considered extremely complex.

The mean squared errors of intensity and phase, denoted

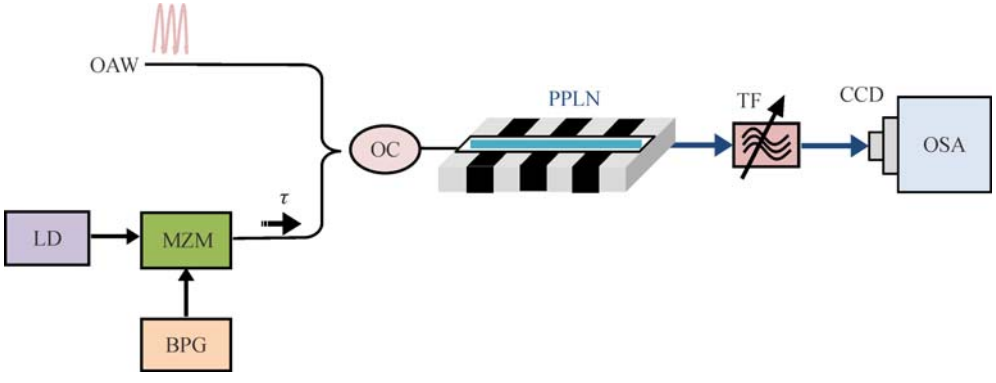

Fig. 1 Schematic of X-FROG measurement for optical arbitrary waveforms using the PPLN waveguide. OAW: optical arbitrary waveform; LD: laser diode; MZM: Mach-Zehnder modulator; BPG: bit pattern generator; OC: optical coupler; PPLN: periodically poled lithium niobate; TF: tunable filter; CCD: charge-coupled device; OSA: optical spectrum analyzer

as A and P, respectively, are introduced to represent the accuracy of the retrieved intensity and phase. Their expressions are given by

$$A = \sqrt{\frac{1}{N}\sum_{i=1}^{N} |\mathrm{abs}[E(t_i)] - \mathrm{abs}[E^k(t_i)]|^2}, \quad (6)$$

$$P = \sqrt{\frac{1}{N}\sum_{i=1}^{N} |\mathrm{angle}[E(t_i)] - \mathrm{angle}[E^k(t_i)]|^2}, \quad (7)$$

where N is the total number of sampling points, i is the certain number of the sampling points, and k is the number of iterations.

4 Simulation results and discussion

The proposed scheme was investigated by a numerical simulation. In the simulation, the central wavelengths of the OAW and the gate pulse were 1550 and 1558 nm, respectively, and the pulse width of the rectangular pulse was 85 fs. The length of the PPLN waveguide was 25 mm, the quasi-phase-matched period was $\Lambda = 5.411$ μm, and the effective interaction area of the nonlinear process was $A_{\mathrm{eff}} = 50\ \mu\mathrm{m}^2$.

4.1 Effects of the complexity of OAW

Figure 2 shows the OAW to be measured of a simple pulse with a TBP value of 1.256. When the complexity of the pulse was 1.256, the retrieved intensity and phase corresponded well to the OAW to be measured, with the values of A and P at 5.4238×10^{-14} and 2.1085×10^{-5}, respectively. The retrieved trace of the arbitrary waveforms to be measured was consistent with the original one.

Figure 3 illustrates a complex pulse. When complexity of the pulse was 11.24, the intensity and phase of the retrieved trace were almost the same as those of the original one, with the values of A and P as 4.5064×10^{-12} and 0.02768, respectively. The retrieved trace of the arbitrary waveforms to be measured was consistent with the original one.

A more complex pulse with a TBP value of 57.59 is shown in Fig. 4. The retrieved intensity correlated well with the original intensity, with a value of $A = 9.2019 \times 10^{-8}$. By contrast, the edge of the retrieved phase did not match with the original phase and the value of P was 0.46891. The retrieved trace of the arbitrary waveforms to be measured was almost consistent with the original one.

The X-FROG traces, the original and retrieved intensities, and the phase of the OAW to be measured in case of different complexities of the pulse are shown in Figs. 2–4,

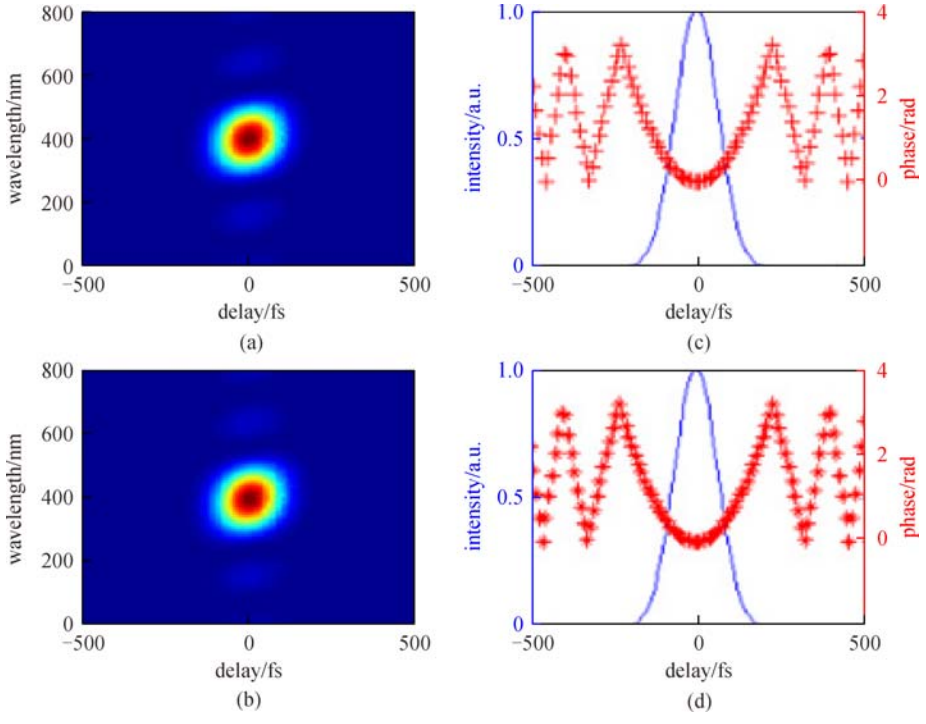

Fig. 2 Measured X-FROG traces of an arbitrary waveform (TBP = 1.256). (a) Original FROG trace of the signal pulse; (b) retrieved FROG trace of the signal pulse; (c) intensity (blue) and phase (red) of the original FROG trace; (d) intensity and phase of the retrieved FROG trace

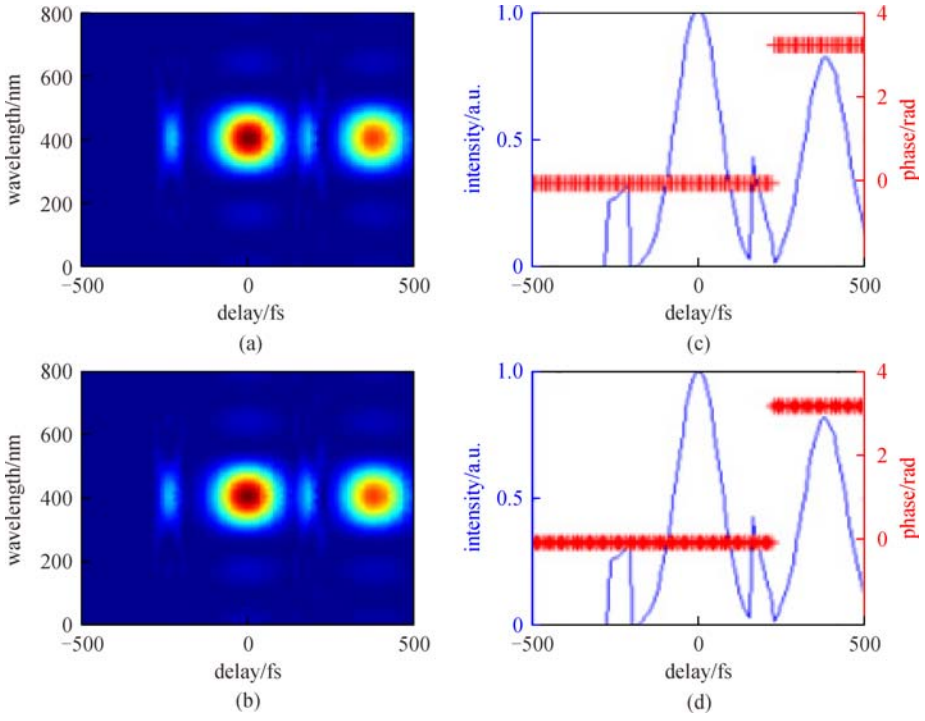

Fig. 3 Measured X-FROG traces of the arbitrary waveform (TBP = 11.24). (a) Original FROG trace of the signal pulse; (b) retrieved FROG trace of the signal pulse; (c) intensity (blue) and phase (red) of the original FROG trace; (d) intensity and phase of the retrieved FROG trace

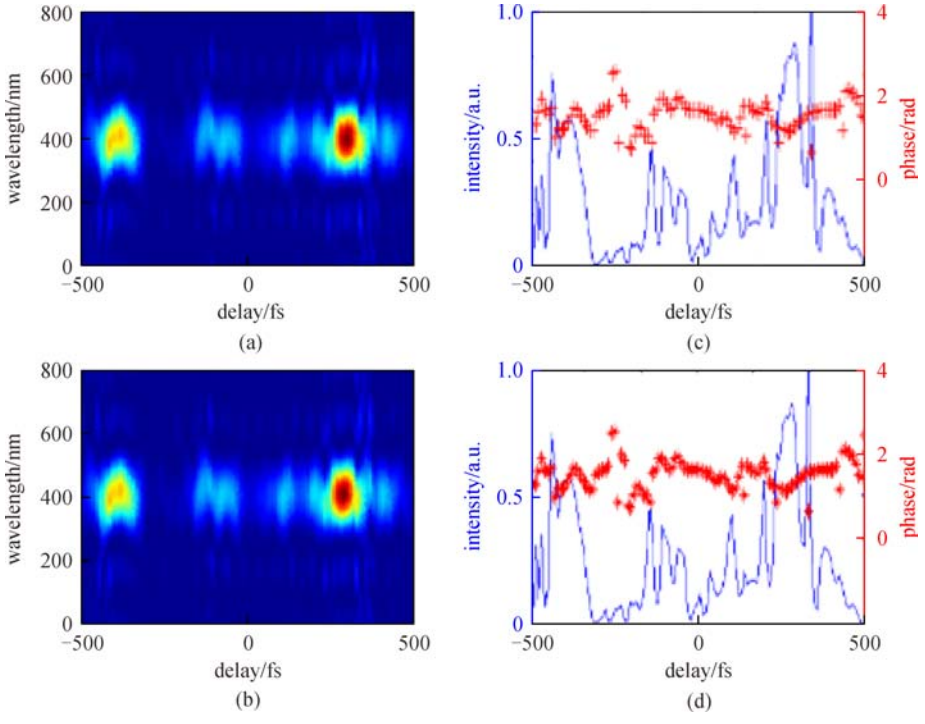

Fig. 4 Measured X-FROG traces of the arbitrary waveform (TBP = 57.59). (a) Original FROG trace of the signal pulse; (b) retrieved FROG trace of the signal pulse; (c) intensity (blue) and phase (red) of the original FROG trace; (d) intensity and phase of the retrieved FROG trace

respectively. The result showed that accuracy decreased with the increase in OAW complexity.

4.2 Effects of different shapes of gate pulses

The OAW to be measured has an arbitrary intensity with a complex phase and a TBP value of 21.59. The original and retrieved intensities and the phases of the OAW to be measured in case of different shapes of the gate pulses are shown in Figs. 5–7, respectively. Figure 5 shows that when the gate pulse is a chirped pulse, the retrieved intensity agrees well with the original intensity, with a value of $A = 8.8438 \times 10^{-10}$. However, the edge of the retrieved phase does not match with the original phase, and the value of P is 0.36837. As shown in Fig. 6, when the gate pulse is a Gaussian pulse, the retrieved intensity agrees well with the original intensity with a value of $A = 8.6723 \times 10^{-10}$. However, the edge of retrieved phase did not match with the original phase, and the value of P is 0.31923. When the shape of the gate pulse is rectangular, the retrieved intensity and phase corresponds well to the OAW to be measured, with the values of A and P given as 6.7923×10^{-10} and 0.18365, respectively (Fig. 7).

Compared with the other two gate pulses, when the shape of the gate pulse is rectangular, the retrieved trace of the arbitrary waveforms to be measured is the most consistent with the original one. Therefore, the gate pulse with a rectangular shape, which has the most accurate characteristics, can be used.

4.3 Effects of the nonlinear length of PPLN waveguide

The OAW to be measured has arbitrary intensity with a complex phase and a TBP value of 21.59. Figure 8 illustrates the original and retrieved intensities and phases of the OAW with different lengths L ($L = 20, 25, 30$ mm) of the PPLN waveguide, respectively. Through a numerical simulation, the values of A and P of the OAW to be measured and the retrieved OAW in the case of different L are presented in Table 1.

The values of A and P are small, and the effect of waveguide length L on the accuracy of the measurement is negligible because the nonlinear effect of the PPLN is strong enough for measurement under the situation of an ideal quasiphase matching (QPM).

4.4 Effects of phase mismatching

The analyses in the previous sections are based on the situation of QPM, which is difficult to achieve in practical applications. In what follows, we discuss the effects of phase mismatching. As shown in Figs. 9(a)–9(h), one of the factors affecting phase mismatching is polarization period Λ.

Figure 9 shows the retrieved intensity and phase of the OAWs to be measured with different polarization period mismatches ($\Delta\Lambda$ = 0, 3, and 6 nm). When the polarization period mismatches are 0, 3, and 6 nm, the phase mismatching Δk_{SFG} are 0, 644.15, and 1298, respectively.

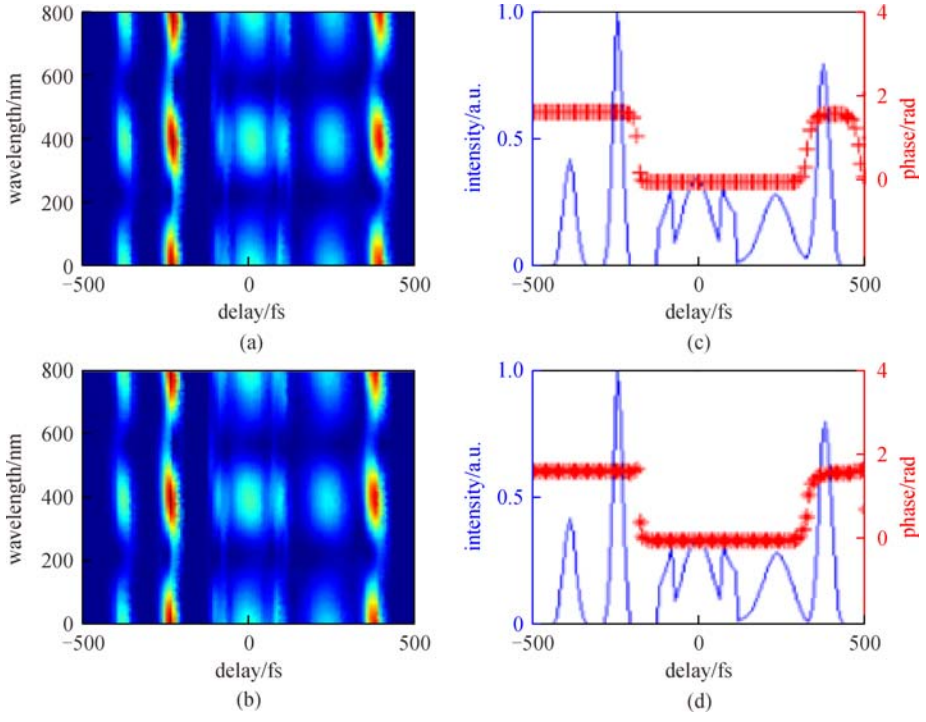

Fig. 5 Measured X-FROG traces of arbitrary waveform (when the gate pulse is chirped). (a) Original FROG trace of the signal pulse; (b) retrieved FROG trace of the signal pulse; (c) intensity (blue) and phase (red) of the original FROG trace; (d) intensity and phase of the retrieved FROG trace

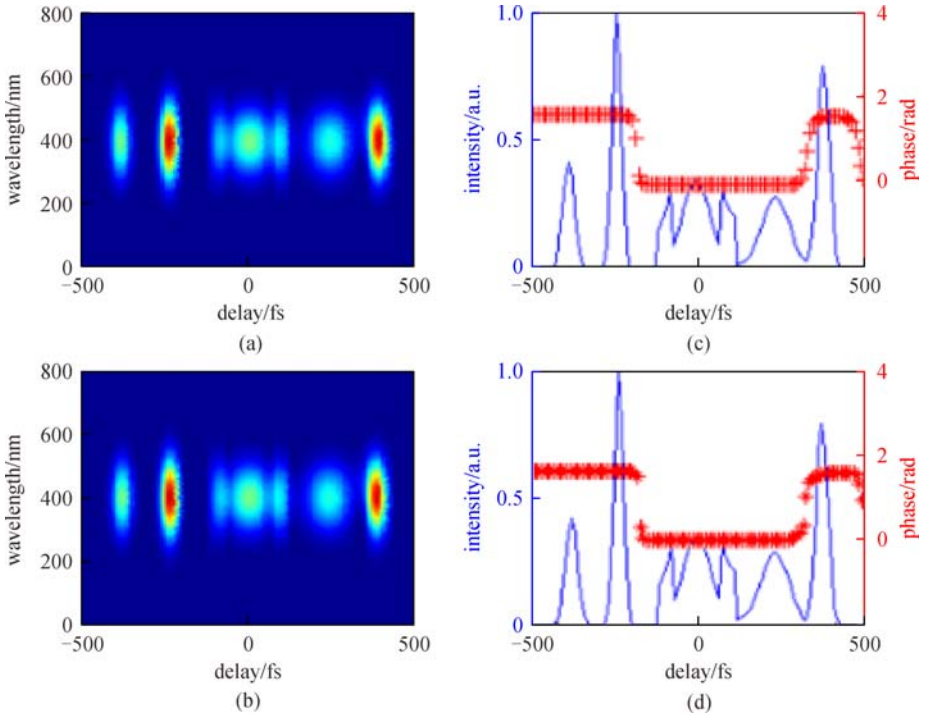

Fig. 6 Measured X-FROG traces of the arbitrary waveform (when the gate pulse is Gaussian). (a) Original FROG trace of the signal pulse; (b) retrieved FROG trace of the signal pulse;(c) intensity (blue) and phase (red) of the original FROG trace; (d) intensity and phase of the retrieved FROG trace

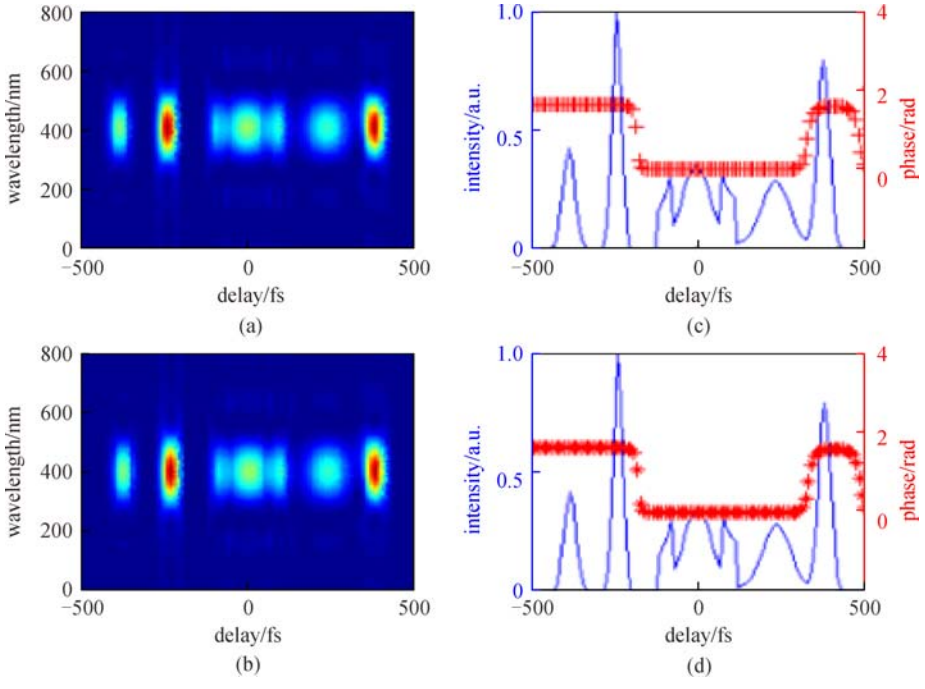

Fig. 7 Measured X-FROG traces of the arbitrary waveform (when the gate pulse is rectangular). (a) Original FROG trace of the signal pulse; (b) retrieved FROG trace of the signal pulse; (c) intensity (blue) and phase (red) of the original FROG trace; (d) intensity and phase of the retrieved FROG trace

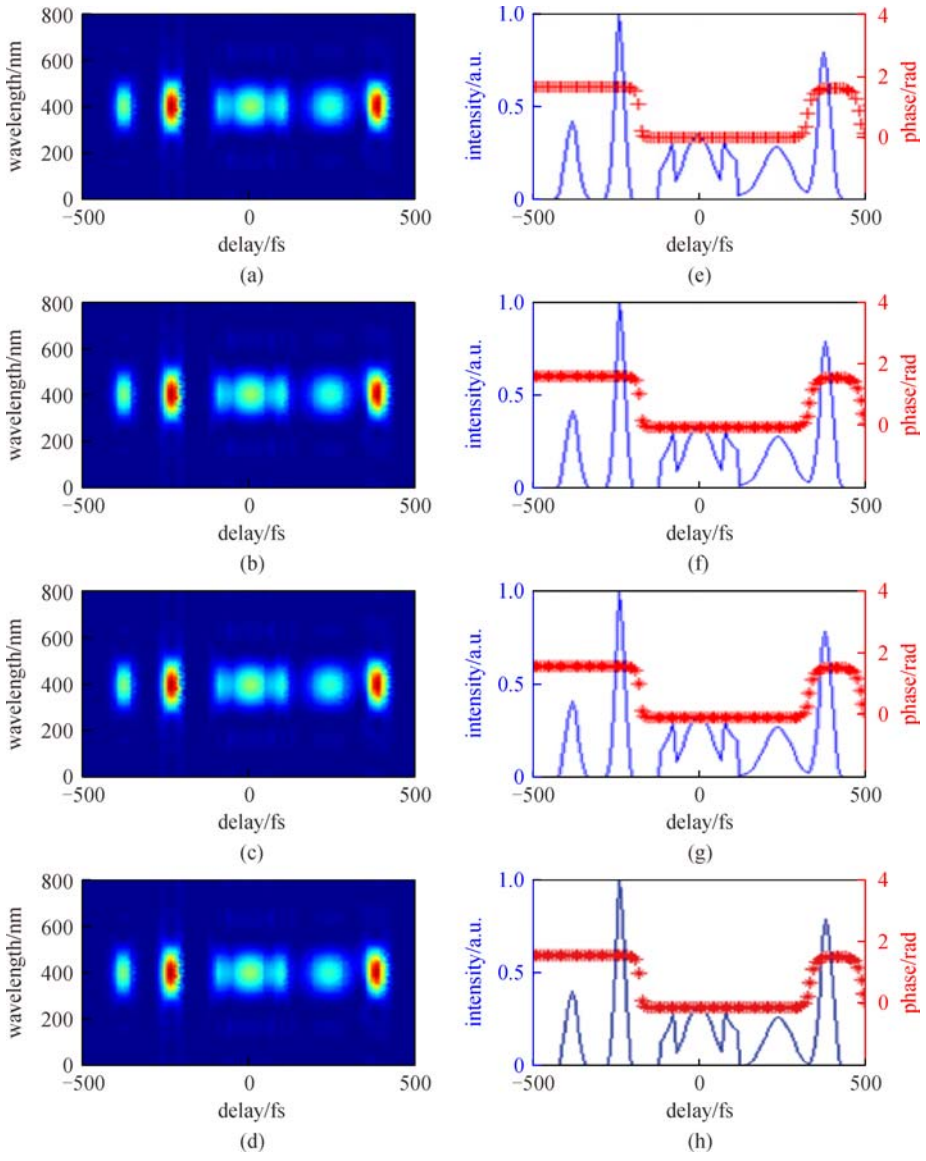

Fig. 8 Measured X-FROG traces of the arbitrary waveform. (a) Original FROG trace of the signal pulse; retrieved FROG trace of the signal pulse when the waveguide length L is (b) 20 mm, (c) 25 mm, and (d) 30 mm; (e) intensity (blue) and phase (red) of the original FROG trace; intensity and phase of the retrieved FROG trace when the waveguide length L is (f) 20 mm, (g) 25 mm, and (h) 30 mm

Table 1 Values of A and P in the case of different L

L/mm	A	P
20	7.4975×10^{-10}	0.18436
25	6.7923×10^{-10}	0.18365
30	7.9048×10^{-10}	0.18633

Through a numerical simulation, the values of A and P of two unknown OAWs in the case of different $\Delta\Lambda$ are shown in Table 2.

Thus, when $\Delta\Lambda$ values are 0, 3, and 6 nm, respectively, the retrieved intensity almost agrees with the original intensity with the magnitude of A up to 10^{-8}. With the increase in polarization period mismatching, the accuracy of measurement decreases. When $\Delta\Lambda$ is close to 6 nm, the phase error is obvious. The intensity and phase errors are relatively small when $\Delta\Lambda$ fails to reach 3 nm.

5 Conclusion

We demonstrated a new X-FROG scheme for OAW measurement based on the PPLN waveguide. The proposed scheme is a powerful and convenient tool for measuring OAWs using the SFG effect of the PPLN

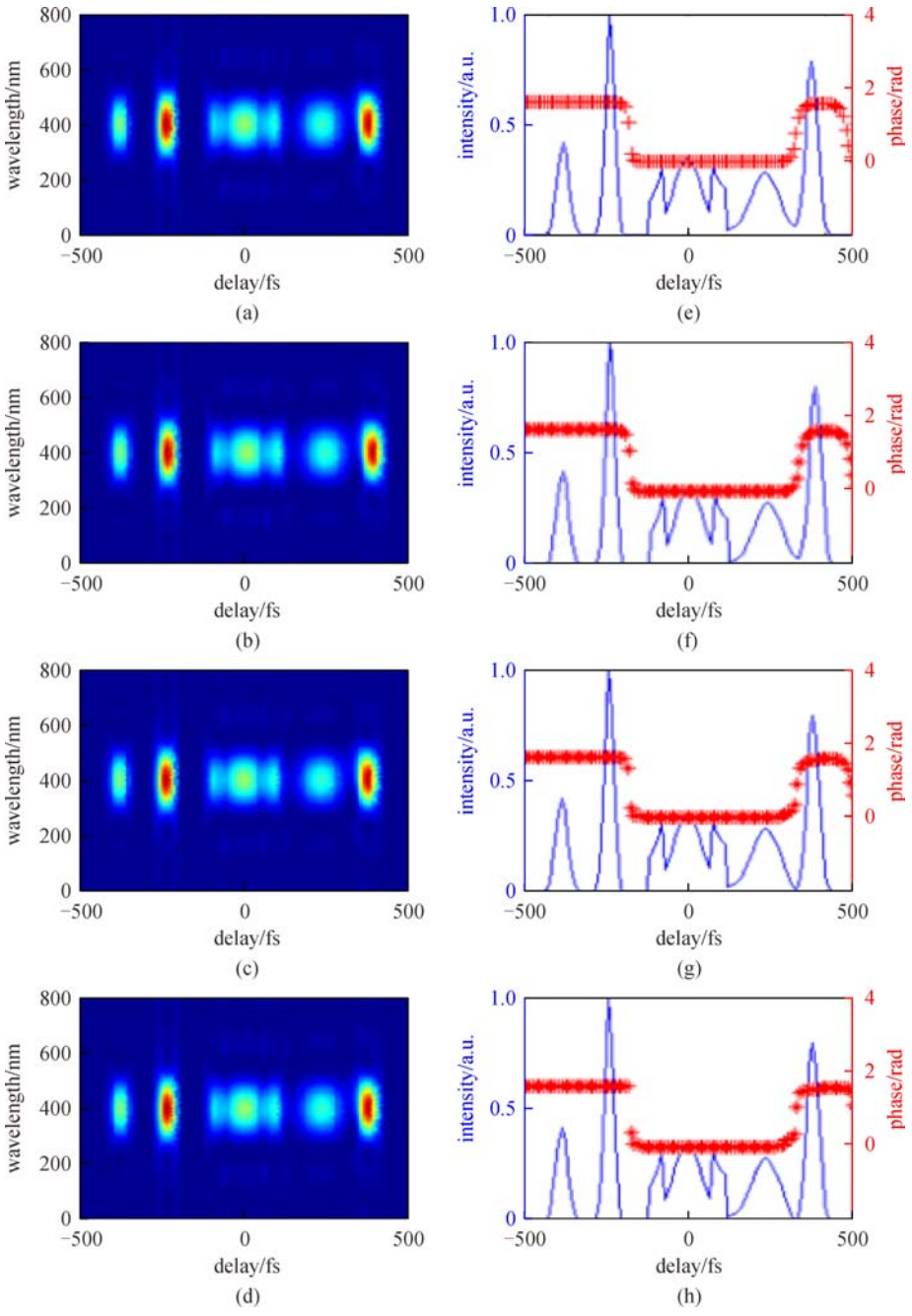

Fig. 9 Measured X-FROG traces of the arbitrary waveform. (a) Original FROG trace of the signal pulse; retrieved FROG trace of the signal pulse when the polarization period mismatched is (b) 0 nm, (c) 3 nm, and (d) 6 nm; (e) intensity (blue) and phase (red) of the original FROG trace; intensity and phase of the retrieved FROG trace when the polarization period mismatching is (f) 0 nm, (g) 3 nm, and (h) 6 nm

Table 2 Values of A and P in the case of different polarization period mismatches $\Delta\Lambda$

$\Delta\Lambda$/nm	A	P
0	6.7923×10^{-10}	0.18365
3	5.9712×10^{-9}	0.25371
6	9.4727×10^{-8}	0.51026

waveguide. We investigated the effects of the complexity of the OAW, shape of the gate pulse, waveguide length, and phase mismatching on accuracy of measurement. The simulation results showed that a rectangular gate pulse achieved few errors. The accuracy of measurement decreased with the increase in OAW complexity and phase mismatching. The effect of the waveguide length on

accuracy of measurement was negligible. The measurement was sufficiently accurate when the phase shift between the polarization period and the quasi-phase-matched period was below 3 nm.

Acknowledgements Related studies were supported by the National Natural Science Foundation of China (Grant No. 61275067), the Natural Science Research Project of Jiangsu University (No. BK2012830) and the open fund of State Key Laboratory of Advanced Optical Communication Systems and Networks, Shanghai Jiao Tong University, China (No. 2015GZKF03006).

References

1. Khan M H, Shen H, Xuan Y, Zhao L, Xiao S, Leaird D E, Weiner A M, Qi M. Ultraboard-bandwidth arbitrary radiofrequency waveform generation with a silicon photonic chip-based spectral shaper. Nature Photonics, 2010, 4(2): 117–122
2. Ho Y Y, Qian L. Dynamic arbitrary waveform shaping in a continuous fiber. Optics Letters, 2008, 33(11): 1279–1281
3. Wang C, Yao J. Large time-bandwidth product microwave arbitrary waveform generation using a spatially discrete chirped fiber Bragg grating. Journal of Lightwave Technology, 2010, 28(11): 1652–1660
4. Supradeepa V R, Leaird D E, Weiner A M. Single shot amplitude and phase characterization of optical arbitrary waveforms. Optics Express, 2009, 17(16): 14434–14443
5. Jiang Z, Huang C B, Leaird D E, Weiner A M. Optical arbitrary waveform processing of more than 100 spectral comb lines. Nature Photonics, 2007, 1(8): 463–467
6. Fontaine N K, Geisler D J, Scott R P, He T, Heritage J P, Yoo S J. Demonstration of high-fidelity dynamic optical arbitrary waveform generation. Optics Express, 2010, 18(22): 22988–22995
7. Fatemi F K, Carruthers T F, Lou J W. Characterisation of telecommunications pulse trains by Fourier-transform and dual-quadrature spectral interferometry. Electronics Letters, 2003, 39 (12): 921–922
8. Miao H, Leaird D E, Langrock C, Fejer M M, Weiner A M. Optical arbitrary waveform characterization via dual-quadrature spectral shearing interferometry. Optics Express, 2009, 17(5): 3381–3389
9. Chen C C, Hsieh I C, Yang S D, Huang C B. Polarization line-by-line pulse shaping for the implementation of vectorial temporal Talbot effect. Optics Express, 2012, 20(24): 27062–27070
10. Supradeepa V R, Leaird D E, Weiner A M. Single shot amplitude and phase characterization of optical arbitrary waveforms. Optics Express, 2009, 17(16): 14434–14443
11. Lepetit L, Chériaux G, Joffre M. Linear techniques of phase measurement by femtosecond spectral interferometry for applications in spectroscopy. Journal of the Optical Society of America B, Optical Physics, 1995, 12(12): 2467–2474
12. Ferdous F, Leaird D E, Huang C B, Weiner A M. Dual-comb electric-field cross-correlation technique for optical arbitrary waveform characterization. Optics Letters, 2009, 34(24): 3875–3877
13. Fontaine N K, Scott R P, Heritage J P, Yoo S J B. Near quantum-limited, single-shot coherent arbitrary optical waveform measurements. Optics Express, 2009, 17(15): 12332–12344
14. Geisler D J, Fontaine N K, Scott R P, Paraschis L. Flexible bandwidth arbitrary modulation format, coherent optical transmission system scalable to terahertz BW. In: Proceedings of IEEE 37th European Conference and Exhibition on Optical Communication (ECOC), 2011, 1–3
15. Scott R P, Fontaine N K, Cao J, Okamoto K, Kolner B H, Heritage J P, Yoo S J. High-fidelity line-by-line optical waveform generation and complete characterization using FROG. Optics Express, 2007, 15(16): 9977–9988
16. Tien E K, Sang X Z, Feng Q, Qi S, Boyraz O. Ultrafast pulse characterization by cross-phase modulation in silicon waveguide. In: Proceedings of IEEE Lasers and Electro-Optics Society, 2008, 306–307
17. Xu L, Zeek E, Trebino R. Measuring very complex ultrashort pulses using frequency-resolved optical gating (FROG). Topics in Applied Physics, 2004, 95: 231–264
18. Xu L, Zeek E, Trebino R. Simulations of frequency-resolved optical gating for measuring very complex pulses. Journal of the Optical Society of America B, Optical Physics, 2008, 25(6): 70–80
19. Wong T C, Ratner J, Chauhan V, Cohen J, Vaughan P M, Xu L, Consoli A, Trebino R. Simultaneously measuring two ultrashort laser pulses on a single-shot using double-blind frequency-resolved optical gating. Journal of the Optical Society of America B, Optical Physics, 2012, 29(6): 1237–1244
20. Pang J. Ultrashort pulse measurement based on microstructure fiber. Dissertation for the Doctoral Degree. Beijing: Beijing University of Posts and Telecommunications, 2012
21. Wong T C, Trebino R. Measuring many-picosecond-long ultrashort pulses on a single shot using XFROG and pulse-front tilt. In: Proceedings of Conference on Lasers and Electro-Optics (CLEO), 2013, 1–2
22. Wu P, Yang S. Spectral phase retrieval by dispersion-distorted frequency-resolved optical gating traces. In: Proceedings of Conference on Lasers and Electro-Optics Pacific Rim (CLEO-PR), 2013, 1–2
23. Fontaine N K, Scott R P, Zhou L, Soares F M, Heritage J P, Yoo S J B. Real-time full-field arbitrary optical waveform measurement. Nature Photonics, 2010, 4(4): 248–254
24. Miao H, Yang S D, Langrock C, Roussev R V, Fejer M M, Weiner A M. Ultralow-power second-harmonic generation frequency-resolved optical gating using aperiodically poled lithium niobate waveguides. Journal of the Optical Society of America B, Optical Physics, 2008, 25(6): A41–A53
25. Kane D J, Rodriguez G, Taylor A J, Clement T S. Simultaneous measurement of two ultrashort laser pulses from a single spectrogram in a single shot. Journal of the Optical Society of America B, Optical Physics, 1997, 14(4): 935–943
26. Geisler D J, Fontaine N K, He T, Scott R P, Paraschis L, Heritage J P, Yoo S J. Modulation-format agile, reconfigurable Tb/s transmitter based on optical arbitrary waveform generation. Optics Express, 2009, 17(18): 15911–15925

Chenwenji Wang is currently a third-year postgraduate student of Nanjing University of Posts and Telecommunications majoring in industrial engineering. Her research direction is optical communication. Her academic area is the highly efficient wavelength conversion in SOI waveguides. Her research consists of five parts, namely, research problems and significance, theoretical bases of the study, methodology, results, and innovation and limitations of the study.

Peili Li received the B.S. degree in physics from Wuhan University, Wuhan, China, in 1996, the M.Sc. degree in physical electronics from the Institute of Laser Technology and Engineering, and the Ph.D. degree from the Department of Optoelectronics Engineering in Huazhong University of Science and Technology, Wuhan, China, in 2000. She worked toward Postdoctor in Wuhan National Laboratory for Optoelectronics in 2007. Now she is working in Nanjing University of Posts and Telecommunications. Her research interests are optoelectronic devices, fiber communication systems, and numerical modeling and simulation of semiconductor optical devices.